Photon structure functions at small x in holographic QCD

Akira Watanabe[a], Hsiang-nan Li[a,b,c]

[a]*Institute of Physics, Academia Sinica, Taipei, Taiwan 115, Republic of China*
[b]*Department of Physics, National Tsing-Hua University, Hsinchu, Taiwan 300, Republic of China*
[c]*Department of Physics, National Cheng-Kung University, Tainan, Taiwan 701, Republic of China*

Abstract

We investigate the photon structure functions at small Bjorken variable x in the framework of the holographic QCD, assuming dominance of the Pomeron exchange. The quasi-real photon structure functions are expressed as convolution of the Brower-Polchinski-Strassler-Tan (BPST) Pomeron kernel and the known wave functions of the U(1) vector field in the five-dimensional AdS space, in which the involved parameters in the BPST kernel have been fixed in previous studies of the nucleon structure functions. The predicted photon structure functions, as confronted with data, provide a clean test of the BPST kernel. The agreement between theoretical predictions and data is demonstrated, which supports applications of holographic QCD to hadronic processes in the nonperturbative region. Our results are also consistent with those derived from the parton distribution functions of the photon proposed by Glück, Reya, and Schienbein, implying realization of the vector meson dominance in the present model setup.

Keywords: Deep inelastic scattering, Gauge/string correspondence, Pomeron, Linear collider

1. Introduction

A photon is a fundamental particle, instead of a nonperturbative composite like hadrons. However, an energetic photon can fluctuate into quark-antiquark pairs, which further radiate gluons, in a hard scattering process. Hence, investigations on the photon structure have served as alternative tests of perturbative approaches to QCD over recent decades. The authors in Refs. [1, 2] first discussed the feasibility of the electron-photon deep inelastic scattering (DIS) and estimated its cross section, whose measurements, such as those conducted at the LEP, provided valuable information of the photon structure functions. After Witten first evaluated the leading-order QCD corrections [3], many elaborated higher-order calculations based on perturbative QCD had been performed [4–10], and the next-to-next-to-leading-order results were available [11]. The consistency between experimental data and theoretical results has strongly supported the reliability of the perturbative calculations in QCD. The picture of the photon structure becomes very different in the kinematic region with a small Bjorken variable x. A photon can fluctuate into vector mesons, so hadronic contributions are not negligible to electron-photon DIS as $x < 0.1$ in general. The hadronic component dominates as $x < 0.01$, and a photon can be regarded as a hadron rather than a point-like object. Effective models are then appropriate for studies of the photon structure functions in this region.

The holographic QCD based on the AdS/CFT correspondence [12–14] is one of the effective models. The AdS/CFT correspondence implies that one can analyze a gauge-theory process at strong coupling in the ordinary Minkowski space by means of the corresponding gravity theory at weak coupling in the higher dimensional AdS space. Since Maldacena first proposed this correspondence, its applications to QCD processes have been attempted intensively [15–22], in which the QCD scale Λ_{QCD} is introduced and the conformal invariance is broken. In particular, phenomenological applications in hadron physics to, e.g., mass spectra, form factors, high-energy scattering processes, and so on, are quite successful.

In this letter we will investigate the photon structure functions at small x, adopting the Pomeron exchange picture in the framework of the holographic QCD. A Pomeron is considered as a color singlet gluonic state composed of multi-gluon exchanges. It has been known that cross sections for various high-energy scattering processes are well described in this picture [23]. A Pomeron in QCD corresponds to a reggeized graviton in the gravity theory in the five-dimensional AdS space. The authors in Ref. [24] evaluated the graviton exchange, and proposed the Brower-Polchinski-Strassler-Tan (BPST) Pomeron kernel. The elaborated analysis in Ref. [25–30] has indicated that applications of this kernel to the nucleon structure functions at small x led to results well consistent with data [31–33].

Following the same formalism, we will express the photon structure functions at small x as convolution of the BPST kernel with the wave functions of the incident and target photons in the 5th dimension. Most parameters in the BPST kernel have been fixed in the previous studies of the nucleon structure functions [32, 33]. The known five-dimensional U(1) vector field will be adopted for the photon wave functions, which couple to leptons at the ultraviolet (UV) boundary. That is, we do not need approximations or models to describe the incident and target particles here, in contrast to the case of the nucleon DIS. Therefore, our study of the photon structure functions involves
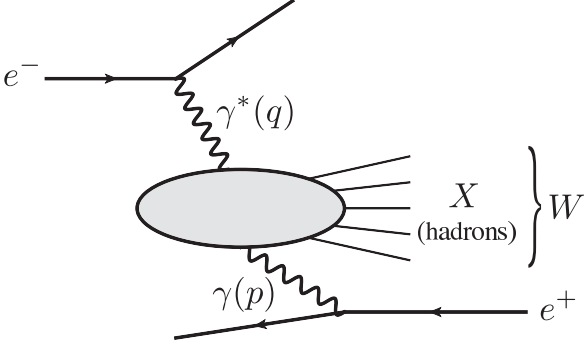
Figure 1: Deeply inelastic electron-photon scattering process, where the bubble represents a parton density of the target photon.

only a single free parameter, which appears as an overall coefficient for the cross section. The model dependence is then reduced, and the predicted photon structure functions, as confronted with data, serve as a clean check of the validity of the BPST kernel. It will be demonstrated that our results for the photon structure function $F_2^\gamma(x, Q^2)$ are in agreement with the LEP data, though available data at small x are limited. In addition, our results are also consistent with those obtained from the parton distribution functions (PDFs) of the photon proposed by Glück, Reya, and Schienbein [34]. Because they included the hadronic component in the photon PDFs, which dominates at small x, this consistency may imply realization of the vector meson dominance in the present setup. Our predictions for the photon structure functions at very low x can be tested at future linear colliders.

2. Kinematics and model setup

The electron-photon DIS $e\gamma \to eX$ is schematically shown in Fig. 1, where q and p are the four-momenta of the probe and target photons, respectively, and W represents the invariant mass of the hadronic final state. The associated differential cross section is expressed in terms of the two structure functions $F_2^\gamma(x, Q^2)$ and $F_L^\gamma(x, Q^2)$ as

$$\frac{d^2\sigma_{e\gamma \to eX}}{dxdQ^2} = \frac{2\pi\alpha^2}{xQ^4} \left\{ \left[1 + (1-y)^2 \right] F_2^\gamma \left(x, Q^2 \right) - y^2 F_L^\gamma \left(x, Q^2 \right) \right\}, \quad (1)$$

where α is the fine structure constant, y is the inelasticity, and the Bjorken scaling variable x is defined as

$$x = \frac{Q^2}{Q^2 + W^2 + P^2}, \quad (2)$$

with $Q^2 = -q^2$ and $P^2 = -p^2$. We consider the small x region with the target being a quasi-real photon, namely, the kinematic region of $W^2 \gg Q^2 \gg P^2$, in which the Bjorken variable can be approximated by $x \approx Q^2/W^2$. The vector meson dominance model [35] appropriate in this region implies that the target photon may behave like a vector meson rather than a point particle, and suggests the application of the Pomeron exchange picture to this process.

The photon structure functions in Eq. (1) are given in the five-dimensional AdS space by [27, 28],

$$F_i^\gamma(x, Q^2) = \frac{\alpha g_0^2 \rho^{3/2} Q^2}{32\pi^{5/2}} \int dz dz' P_{13}^{(i)}(z, Q^2) P_{24}(z', P^2)$$
$$\times (zz') \text{Im}[\chi_c(W^2, z, z')], \quad (3)$$

with $i = 2, L$, where the adjustable parameters g_0^2 and ρ control the magnitude and the energy dependence of the structure functions, respectively. The imaginary part of the BPST Pomeron kernel [24, 28]

$$\text{Im}[\chi_c(W^2, z, z')] = e^{(1-\rho)\tau} e^{-[\log^2 z/z')/\rho\tau]} / \sqrt{\tau}, \quad (4)$$

with the conformal invariant

$$\tau = \log(\rho zz' W^2 /2), \quad (5)$$

arises from the single-Pomeron/graviton exchange.

The overlap functions $P_{13}(z)$ and $P_{24}(z')$, describing the density distributions of the incident and target particles in the AdS space, respectively, obey the normalization condition $\int dz P_{ij}(z) = 1$ in the on-shell case. They depend on the particle virtualities Q^2 and P^2 in the present study with off-shell photons. $P_{13}^{(L)}(z, Q^2)$ denotes the wave function of the longitudinally polarized photon, and $P_{24}(z', P^2)$ takes the form the same as $P_{13}^{(2)}(z, Q^2)$. The massless 5D U(1) vector field, satisfying the Maxwell equation in the five-dimensional AdS background spacetime, can be identified as the physical photon at the UV boundary. We adopt the wave function of this field for the overlap functions, which are then written as [36]

$$P_{13}^{(2)}(z, Q^2) = Q^2 z \left[K_0^2(Qz) + K_1^2(Qz) \right], \quad (6)$$

$$P_{13}^{(L)}(z, Q^2) = Q^2 z K_0^2(Qz). \quad (7)$$

Both $K_0(Qz)$ and $K_1(Qz)$, the modified Bessel functions of the second kind, diverge at the origin and vanish at large Qz, consistent with the fact that a photon is a non-normalizable mode, and can penetrate into the larger z, i.e., infrared (IR) region at low Q. Namely, Eq. (6) exhibits the feature that a quasi-real photon propagates into the bulk of the AdS space, while keeping a substantial component in the UV region even at small x.

In the considered region with $10^{-5} \leq x \leq 10^{-2}$ and 1 GeV^2 $\leq Q^2 \leq 10$ GeV^2, nonperturbative hadronic contribution to the structure functions may become important. We employ the modified kernel [24, 31]

$$\text{Im}[\chi_{mod}(W^2, z, z')] \equiv \text{Im}[\chi_c(W^2, z, z')]$$
$$+ \mathcal{F}(z, z', \tau) \text{Im}[\chi_c(W^2, z, z_0^2/z')], \quad (8)$$

$$\mathcal{F}(z, z', \tau) = 1 - 2\sqrt{\rho\pi\tau} e^{\eta^2} \text{erfc}(\eta), \quad (9)$$

$$\eta = \left(-\log \frac{zz'}{z_0^2} + \rho\tau \right) / \sqrt{\rho\tau}, \quad (10)$$

where the first term on the right-hand side of Eq. (8) is the conformal kernel, and the second term represents the additional confinement effect. The adjustable parameter $z_0 \sim 1/\Lambda_{\text{QCD}}$, being of order of the QCD scale, governs the strength of the

confinement effect. The factor $\mathcal{F}$, running from 1 to −1 for fixed z and z', as τ increases from zero to infinity, suppresses the structure functions at large W^2. That is, the confinement effect intensifies at small x for fixed Q^2. Strictly speaking, there must be modification of the background metric as the confinement effect is not negligible, which may lead to a more complicated kernel with more parameters. However, it has been also observed [33] that the modified kernel in Eq. (8) well reproduces the data for the nucleon structure functions at small x, which are typical nonperturbative quantities.

3. Numerical results

We take the parameter sets for the BPST kernels obtained in Ref. [33] with $z_0 = 4.25\,\text{GeV}^{-1}$ or $z_0 = 6\,\text{GeV}^{-1}$ in the modified kernel case, which has been demonstrated to well reproduce the data of the nucleon structure functions at small x. Since a photon is a non-normalizable mode, the overall coefficient g_0^2 in Eq. (3) is an unknown, and has to be tuned to fit the absolute magnitude of data. The available data of the real photon structure functions at small x are still quite limited. We consider 9 data points from the OPAL collaboration at LEP [37] with $x \le 0.025$, and determine $g_0^2 = 17.51$ and 49.01 for the conformal and modified kernels, respectively. The invariant mass squared P^2 of the target photon should be small enough, but cannot be exactly zero in practice. Events in the region with $P^2 \sim \mathcal{O}(0.01)\,\text{GeV}^2$ have been measured (for details, see review papers [38, 39] and references therein), so $P^2 = 0.01\,\text{GeV}^2$ is assumed here [34].

We explain the treatment of the conformal invariant τ, which appears in the kernels in Eqs. (4) and (8). Straightforward integrations collect the contribution from the region of small z and z', where the photon distributions concentrate, yielding a negative τ, i.e., an imaginary piece in the kernels. A simple resolution of this difficulty is to restrict z and z' in the region, where τ remains positive. We refer to this prescription as scheme 1. Another way is to set z and z' in the definition of τ to their average values defined by

$$\bar{z} \equiv \frac{\int dz z^2 P_{13}^{(i)}\left(z, Q^2\right)}{\int dz z P_{13}^{(i)}\left(z, Q^2\right)}, \qquad \bar{z}' \equiv \frac{\int dz' z'^2 P_{24}\left(z', P^2\right)}{\int dz' z' P_{24}\left(z', P^2\right)}, \qquad (11)$$

respectively, and regarding the product zz' in Eq. (5) as the characteristic scale $\bar{z}\bar{z}'$ of the kernels. We have verified that this prescription, referred to as scheme 2, works for explaining the data of the nucleon structure functions with the model setup in Ref. [33]. As indicated in Fig. 2, the results for the photon structure function $F_2^\gamma(x, Q^2)$ from these two schemes differ slightly (about few percents) at least in the currently considered kinematic region. We will adopt scheme 2 for the numerical analysis below.

We display in Fig. 3 the predicted x and Q^2 dependencies of the structure function F_2^γ for the quasi-real photon from Eq. (3) with the conformal and modified Pomeron kernels, and those derived from the well-known PDF sets, GRV [40] and GRS [34], at next-to-leading-order accuracy. Both curves from
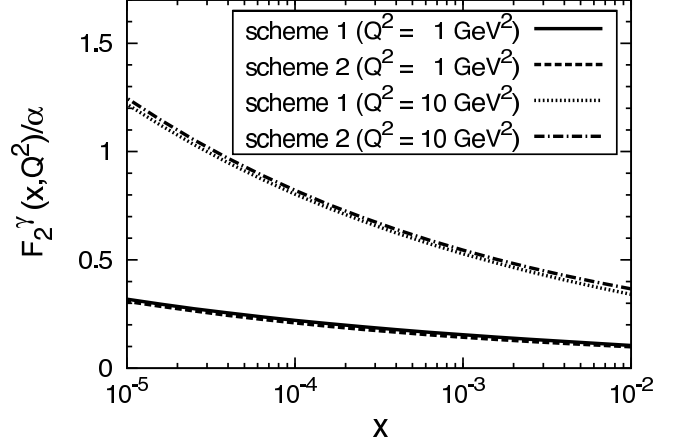

Figure 2: $F_2^\gamma(x, Q^2)$ as a function of x for $Q^2 = 1, 10\,\text{GeV}^2$ derived from schemes 1 and 2 for the treatment of the conformal invariant τ with the modified kernel.

GRV and GRS include the charm-quark contribution in the region with $W \ge 2m_c$. Note that the hadronic contributions to the GRV and GRS PDFs were parameterized via the pion PDFs based on the assumed similarity between the vector meson and the pion, and that the validity of the parameterizations in Refs. [40, 34] is limited to the range $Q^2 > 0.5\,\text{GeV}^2$ and $x > 10^{-5}$. It is seen in Fig. 3 that all the above curves basically match the data available for $x > 10^{-3}$, and then ascend with different slopes as x decreases, a feature attributed to the Pomeron exchange. Future data will further discriminate the different predictions at small $x < 10^{-3}$. To be precise, the results from the modified kernel with $z_0 = 6\,\text{GeV}^{-1}$ and from the conformal kernel fit the data equally well based on χ^2 per degree of freedom, and slightly better than those from the modified kernel with $z_0 = 4.25\,\text{GeV}^{-1}$. If we focus on the region with low $Q^2 < 10\,\text{GeV}^2$ and small $x < 0.01$, and tune the only parameter g_0^2 again, the modified kernel with $z_0 = 6\,\text{GeV}^{-1}$ gives the best fit to the data.

The results from the conformal kernel (GRV PDFs) show the weakest (strongest) x dependence, and those from the GRS PDFs show the moderate x dependence. The obvious difference between the GRV and GRS predictions in the small x region, and their comparison with the OPAL data have been discussed in Ref. [41]. The curves from the modified kernel exhibit the similar x dependence and the stronger Q^2 dependence compared to those from the conformal kernel. The former are closer to the GRS curves compared to the latter, and coincide with the GRS curves as indicated in the first two panels of Fig. 3. It is straightforward to find that the hadronic component in the GRS photon PDFs dominates at small x, about 90% (80%) of the total contribution to F_2^γ for $Q^2 = 1$ (10) GeV^2. This consistency may imply realization of the vector meson dominance in the present model setup.

It is found that the difference between the curves from the modified kernel and from the conformal kernel becomes larger, as Q^2 increases and as x decreases. Note that the two kernels in Eqs. (4) and (8) have been treated as independent models,
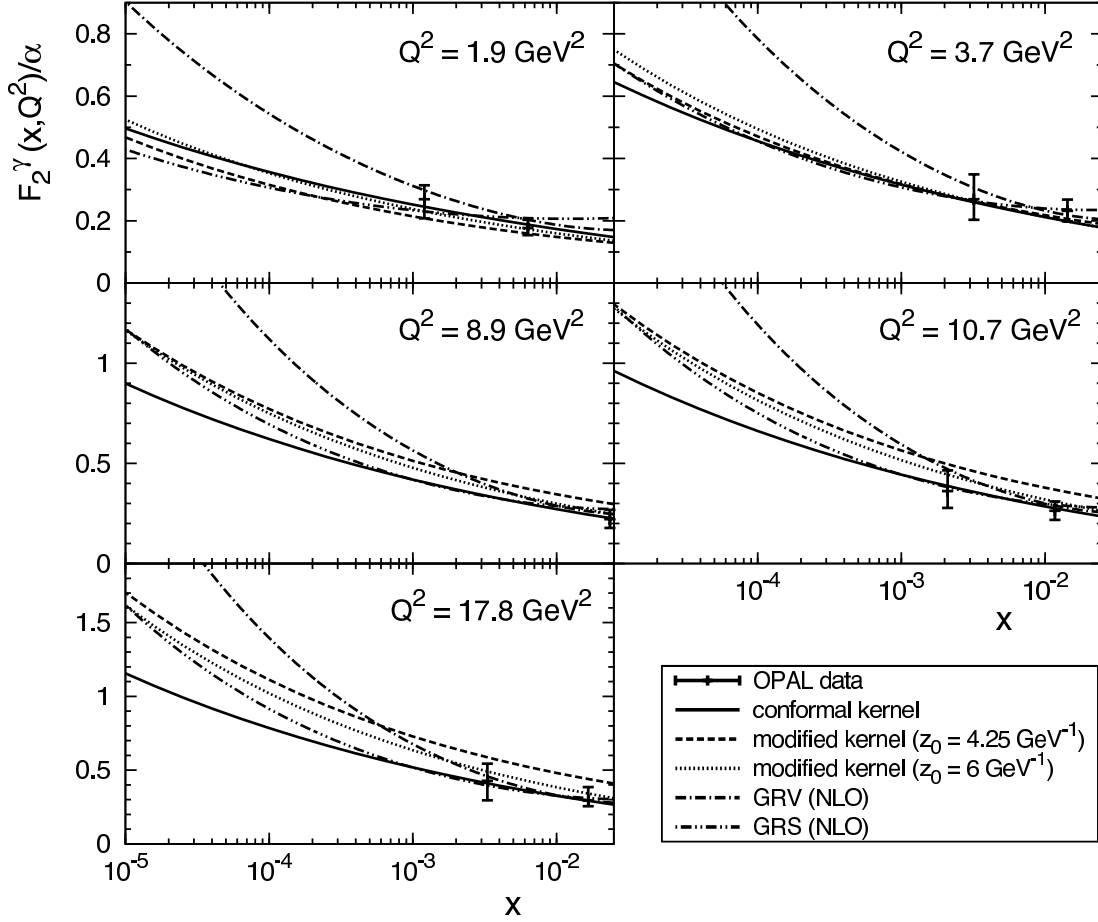
Figure 3: $F_2^\gamma(x, Q^2)$ as a function of x for various Q^2, and its comparison with the data from the OPAL Collaboration [37]. In each panel, the solid, dashed, and dotted curves are from our calculations. The dash-dotted and dashed double-dotted curves represent the GRV [40] and GRS [34] predictions, respectively.

and their adjustable parameters have been fixed separately [33]. It has been known that the different parameter sets are needed to well describe the data of the nucleon structure function F_2^p with the two kernels in the $Q^2 < 10$ GeV^2 region. Therefore, the growing difference does not imply that the confinement effect from the second term in Eq. (8) increases with Q^2. It does not imply either that this term is positive in the small x region. Choosing a common parameter set for both the conformal and modified kernels, we indeed see that the relative difference between the resultant photon structure functions reduces, and the latter become lower than the former as x decreases. That is, the confinement effect is weakened at high Q^2, and the second term in Eq. (8) remains negative at small x. Nevertheless, the resultant photon structure functions approach to each other at high Q^2 more slowly than in Ref. [31] due to the different treatments of density distributions of the involved particles[1].

The agreement of the results from the modified kernel with the data can be further improved by considering the number of active quark flavors f involved in the analysis. The target nucleon overlap function is localized in the IR region around $z' \sim 4$ GeV^{-1} [33], so that the heavy quark contribution is suppressed, and we have $f \sim 4$. The target photon overlap function $P_{24}(z', P^2)$ spreads broadly from the UV region to the IR region in the z' space, implying the participation of all flavors, i.e., $f = 6$. Because the QCD scale $\Lambda_{QCD} \sim 1/z_0$ decreases with f, the parameter z_0 in the present study may be larger than that fixed in Ref. [33]. We then calculate the structure function F_2^γ, assuming $z_0 = 6$ GeV^{-1} and $g_0^2 = 21.60$, and display the results in Fig. 3 as well. It is observed that the corresponding dotted curves, becoming higher than the dashed ones as $Q^2 = 1.9$ GeV^2, and lower as $Q^2 > 8.9$ GeV^2, agree completely with the OPAL data within errors.

Next we present the x dependence of the ratio of the longitudinal structure function over the transverse structure function, defined as $R_{L/T} = F_L^\gamma(x, Q^2)/F_T^\gamma(x, Q^2)$ with $F_T^\gamma = F_2^\gamma - F_L^\gamma$, in Fig 4. It is found that $R_{L/T}$ increases with x and Q^2 in both cases of the conformal and modified kernels. $R_{L/T}$ seems to be almost constant for the modified kernel with $Q^2 = 1$ GeV^2. These results are qualitatively consistent with those of the nucleon structure functions [33]. It is easy to understand $R_{L/T} < 1$, since the contribution from the longitudinal polarization of the probe photon is suppressed at low Q^2, and the increase of $R_{L/T}$

---

[1]The kernel ratio $r \equiv \mathrm{Im}[\chi_{mod}]/\mathrm{Im}[\chi_c]$, which reflects the detailed difference between the modified and conformal kernels, has been investigated, and its behavior has been shown in Fig. 1 of Ref. [33].
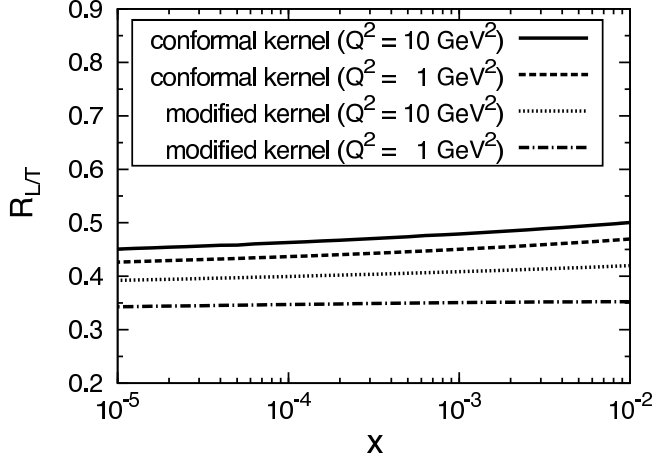
Figure 4: Ratio $R_{L/T} = F_L^\gamma(x, Q^2)/F_T^\gamma(x, Q^2)$ as a function of x for $Q^2 = 1, 10$ GeV^2. The parameter value $z_0 = 4.25$ GeV^{-1} is adopted to obtain the curves from the modified kernel.
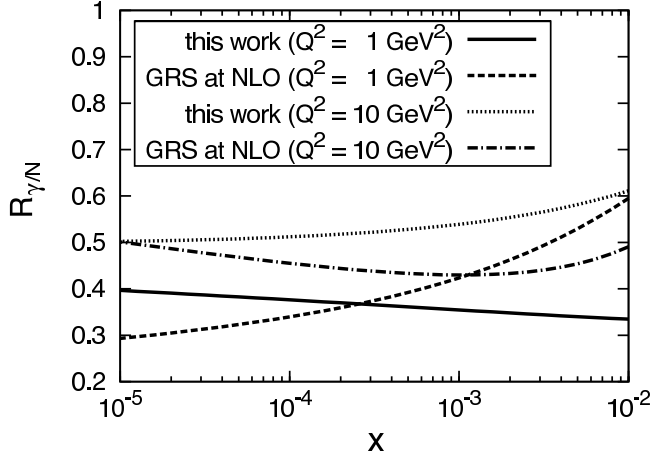

Figure 5: Ratio $R_{\gamma/N} = F_2^\gamma(x, Q^2)/[\alpha F_2^N(x, Q^2)]$ as a function of x for $Q^2 = 1$ and 10 GeV^2, and its comparison with the GRS predictions [34]. $F_2^\gamma(x, Q^2)$ is obtained by employing the modified kernel with $z_0 = 4.25$ GeV^{-1}. $F_2^N(x, Q^2)$ is from Ref. [33], and common to all the curves.

with Q^2, since this contribution increases with Q^2. However, $R_{L/T}$ around 0.4 also indicates that the longitudinal structure function is not negligible in the considered kinematical region.

Finally, we compare the x dependence of the photon structure function F_2^γ with that of the nucleon structure function F_2^N by investigating their ratio $R_{\gamma/N} = F_2^\gamma(x, Q^2)/[\alpha F_2^N(x, Q^2)]$. For $F_2^N(x, Q^2)$, we adopt the results in Ref. [33], which match the HERA data [42] well. As shown in Fig. 5, both curves from our predictions are nearly linear with small slopes. The similar x dependencies of the two structure functions is again attributed to the universal Pomeron kernel in our framework. We also plot the GRS predictions for the ratio $R_{\gamma/N}$ in Fig. 5. Our and GRS predictions are closer to each other for $Q^2 = 10$ GeV^2, because both agree with the data at this scale as indicated in Fig 3. Our and GRS predictions differ significantly for $Q^2 = 1$ GeV^2, especially at $x \sim 10^{-2}$, because the former exhibits a substantial

x dependence, while the latter becomes almost independent of x as $x > 10^{-3}$.

4. Summary

In this letter we have investigated the structure functions F_2^γ and F_L^γ of the quasi-real photon in the region of small Bjorken variable x in a holographic QCD model. They were calculated by convoluting the BPST Pomeron kernel with the wave functions of the U(1) vector field in the five-dimensional AdS space. Two of three adjustable parameters of the kernel have been fixed in the previous studies on the nucleon DIS, so only a single overall parameter was left free, and tuned to fit the absolute magnitude of the experimental data. The predicted dependencies of $F_2^\gamma(x, Q^2)$ on x and Q^2 are in agreement with the OPAL data, implying the predictive power of the present model setup, and that the Pomeron exchange picture can describe general DIS processes at small x reasonably.

We then compared our results with the structure functions derived from the GRV and GRS PDF sets of the photon, and the consistency with the latter was also observed. Since the hadronic component in the photon PDFs dominates at small x, this consistency may be regarded as realization of the vector meson dominance. It is known that the vector meson dominance model well accommodates experimental data involving quasi-real photons, whose mechanism is, however, not completely understood due to its nonperturbative origin. The wave functions for a quasi-real photon proposed in Eq. (6), with broad distribution in the z space, can overlap with the ρ meson wave function significantly. It is likely that the quasi-real photon wave function and the ρ meson wave function, as convoluted with the universal Pomeron kernel, yield similar cross sections. Then holographic models might have provided an alternative viewpoint to realize the vector meson dominance mechanism. Future linear colliders, such as the planned International Linear Collider, will help fully understand the nature of a photon, which is one of the most fundamental issues in high energy physics.

References

[1] S. J. Brodsky, T. Kinoshita, H. Terazawa, Phys.Rev.Lett. 27 (1971) 280.
[2] T. Walsh, Phys.Lett. B36 (1971) 121.
[3] E. Witten, Nucl.Phys. B120 (1977) 189.
[4] C. Llewellyn Smith, Phys.Lett. B79 (1978) 83.
[5] W. A. Bardeen, A. J. Buras, Phys.Rev. D20 (1979) 166.
[6] D. Duke, J. Owens, Phys.Rev. D22 (1980) 2280.
[7] I. Antoniadis, G. Grunberg, Nucl.Phys. B213 (1983) 445.
[8] M. Gluck, E. Reya, Phys.Rev. D28 (1983) 2749.
[9] M. Fontannaz, E. Pilon, Phys.Rev. D45 (1992) 382.

[10] M. Gluck, E. Reya, A. Vogt, Phys.Rev. D45 (1992) 3986.

[11] S. Moch, J. Vermaseren, A. Vogt, Nucl.Phys. B621 (2002) 413.

[12] J. M. Maldacena, Adv.Theor.Math.Phys. 2 (1998) 231.

[13] S. Gubser, I. R. Klebanov, A. M. Polyakov, Phys.Lett. B428 (1998) 105.

[14] E. Witten, Adv.Theor.Math.Phys. 2 (1998) 253.

[15] M. Kruczenski, D. Mateos, R. C. Myers, D. J. Winters, JHEP 0307 (2003) 049.

[16] M. Kruczenski, D. Mateos, R. C. Myers, D. J. Winters, JHEP 0405 (2004) 041.

[17] T. Sakai, S. Sugimoto, Prog.Theor.Phys. 113 (2005) 843.

[18] T. Sakai, S. Sugimoto, Prog.Theor.Phys. 114 (2005) 1083.

[19] D. T. Son, M. A. Stephanov, Phys.Rev. D69 (2004) 065020.

[20] J. Erlich, E. Katz, D. T. Son, M. A. Stephanov, Phys.Rev.Lett. 95 (2005) 261602.

[21] L. Da Rold, A. Pomarol, Nucl.Phys. B721 (2005) 79.

[22] J. Erdmenger, N. Evans, I. Kirsch, E. Threlfall, Eur.Phys.J. A35 (2008) 81.

[23] A. Donnachie, P. Landshoff, Phys.Lett. B296 (1992) 227.

[24] R. C. Brower, J. Polchinski, M. J. Strassler, C.-I. Tan, JHEP 0712 (2007) 005.

[25] L. Cornalba, M. S. Costa, J. Penedones, JHEP 0709 (2007) 037.

[26] L. Cornalba, M. S. Costa, Phys.Rev. D78 (2008) 096010.

[27] R. C. Brower, M. J. Strassler, C.-I. Tan, JHEP 0903 (2009) 050.

[28] R. C. Brower, M. J. Strassler, C.-I. Tan, JHEP 0903 (2009) 092.

[29] L. Cornalba, M. S. Costa, J. Penedones, Phys.Rev.Lett. 105 (2010) 072003.

[30] L. Cornalba, M. S. Costa, J. Penedones, JHEP 1003 (2010) 133.

[31] R. C. Brower, M. Djuric, I. Sarcevic, C.-I. Tan, JHEP 1011 (2010) 051.

[32] A. Watanabe, K. Suzuki, Phys.Rev. D86 (2012) 035011.

[33] A. Watanabe, K. Suzuki, Phys.Rev. D89 (2014) 115015.

[34] M. Gluck, E. Reya, I. Schienbein, Phys.Rev. D60 (1999) 054019.

[35] J. Sakurai, Annals Phys. 11 (1960) 1.

[36] J. Polchinski, M. J. Strassler, JHEP 0305 (2003) 012.

[37] G. Abbiendi, et al., Eur.Phys.J. C18 (2000) 15.

[38] R. Nisius, Phys.Rept. 332 (2000) 165.

[39] M. Krawczyk, A. Zembrzuski, M. Staszel, Phys.Rept. 345 (2001) 265.

[40] M. Gluck, E. Reya, A. Vogt, Phys.Rev. D46 (1992) 1973.

[41] M. Gluck, E. Reya, I. Schienbein, Phys.Rev. D64 (2001) 017501.

[42] F. Aaron, et al., JHEP 1001 (2010) 109.